Supporting Information for:

Controlling Hydricity of Adsorbed Catalysts with Applied Electric Fields

H. Ray Kelly,[1] Pablo E. Videla,[1] Clifford P. Kubiak,[2] Tianquan Lian,[3] and Victor S. Batista[1,*]

[1)] *Department of Chemistry, Yale University, New Haven, Connecticut 06520, United States*
[2)] *Department of Chemistry and Biochemistry, University of California, San Diego, La Jolla, California 92093, United States*
[3)] *Department of Chemistry, Emory University, Atlanta, Georgia 30322, United States*

Table of Contents

Section S1 – Relationship Between Hydricity, BDFE and pK_a

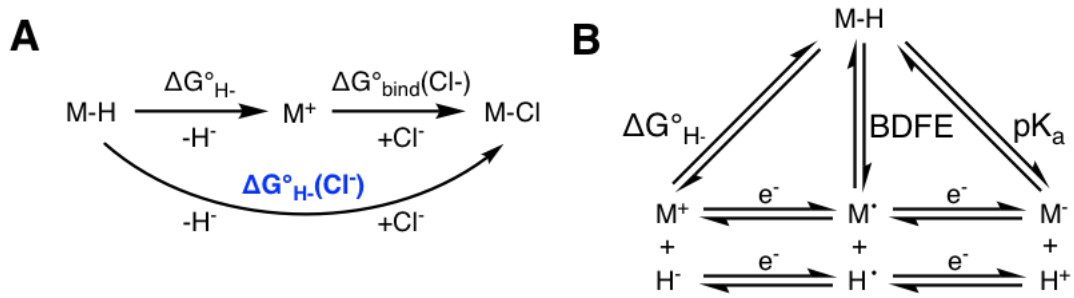

Figure S1. (A) Scheme showing the relationship between the effective hydricity computed in this work, $\Delta G°_{H-}(Cl^-)$ (blue), and the thermodynamic hydricity, $\Delta G°_{H-}$. The effective hydricity also includes the free energy associated with binding a Cl^- ligand to the metal center, $\Delta G°_{bind}(Cl^-)$, and is the most relevant descriptor of hydride transfer behavior in aqueous conditions. (B) Scheme showing the connection between $\Delta G°_{H-}$, bond dissociation free energy (BDFE), and pK_a. These three different types of M-H dissociation free energies are interrelated by the redox potentials of the metal complex and H.

Section S2 - Additional Computational Details

Au (111) Surface Model: A single layer Au (111) model was used to determine the orientation of catalytic adsorbates. This model was generated from a larger gold slab optimized using periodic boundary conditions in the Vienna Ab initio Simulation Program (VASP) version 5.4.[1-4] A bulk optimization of Au was performed using the projector-augmented wave (PAW) method[5, 6] with the Perdew-Berke-Ernzerhof (PBE) exchange-correlation functional[7] and Grimme's DFT-D3 dispersion correction with Becke-Johnson damping.[8, 9] Bulk optimization (including positions, cell shape, and volume) was performed with a 12×12×12 Monkhorst-Pack k-point grid centered at the gamma point, first-order Methfessel-Paxton smearing (σ = 0.2 eV),[10] and a plane wave cutoff energy of 500 eV. The self-consistent energy convergence criterion was 10^{-6} eV, while the ionic relaxation convergence criterion was 10^{-5} eV. The lattice vectors of the optimized bulk structure were used to generate a four layer Au (111) slab with 36 atoms in each layer (i.e. 6×6×4 atoms) and a 40 Å vacuum spacer. The positions of the atoms in the surface structure were optimized, with the bottom two layers frozen to maintain the bulk geometry. For this larger structure, a 1×1×1 k-point grid was used (i.e. gamma point). All other parameters were maintained from the bulk calculation. The top layer of the optimized slab was used to generate the single layer model shown in **Figure S2**. An odd number of Au atoms were included in the model to ensure a singlet multiplicity in the calculations with the adsorbed catalyst. Tests with a two-layer gold model showed no significant difference in the computed reaction energetics despite a substantially greater computational cost, so a one-layer model was used in all reported calculations.

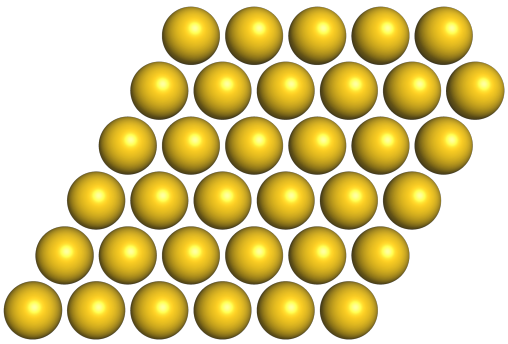

Figure S2. Top view of single layer Au (111) model

Calculations of Hydricity: The effective hydricity, $\Delta G°_{H-}(Cl^-)$, computed in this work corresponds to the change in free energy for the exchange of a hydride anion for a chloride:

$$\mathbf{M\text{-}H + Cl^- (aq) \rightarrow M\text{-}Cl + H^- (aq)}$$

To calculate the free energy of this reaction, we used a thermodynamic cycle including a compound of known hydricity, specifically the unsubstituted **[Ir-bpy-H]**$^+$ analogue (**Figure S3**). The aqueous hydricity of this complex was experimentally measured to be 27.0 kcal/mol.[11] Similar free energy cycles have been used in previous DFT calculations of hydricity to ensure accurate thermodynamic quantities, and avoid complications arising from the need to compute the solvation free energy of a hydride anion.[12, 13] In essence, the experimental reference value serves as an absolute scale to which the relative reaction free energies can be compared.

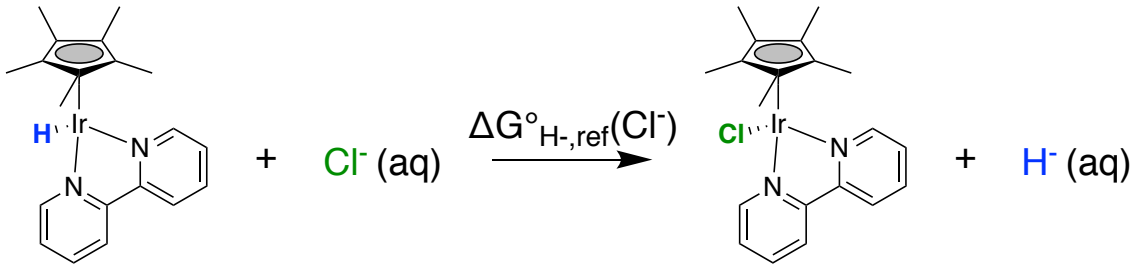

Figure S3. Reference reaction used for DFT calculations of hydricity ($\Delta G°_{H-,ref}(Cl^-)$ = 27.0 kcal/mol).

The thermodynamic cycle used to compute the unknown hydricity value $\Delta G°_{H-}(Cl^-)$ consists of three reactions (**Figure S4**). First, we used DFT to compute $\Delta G°_{HT}$, the free energy of hydride transfer with the reference complex behaving as a hydride acceptor and the complex of interest acting as a hydride donor. This value can be added to the experimentally reported reference hydricity, $\Delta G°_{H-,ref}(Cl^-)$, to give the hydricity of the molecule of interest. An example reaction scheme for determining the hydricity of the methoxy substituted complex is shown in **Figure S4**. All hydricity calculations followed the same series of reactions shown in **Figure S4** with the methoxy substituted complex replaced by the complex of interest. **Section S3** discusses the benchmarking calculations used to ensure that this process gave accurate values of aqueous hydricities.

$$\Delta G°_{H-}(Cl^-) = \Delta G°_{HT} + \Delta G°_{H-,ref}(Cl^-)$$

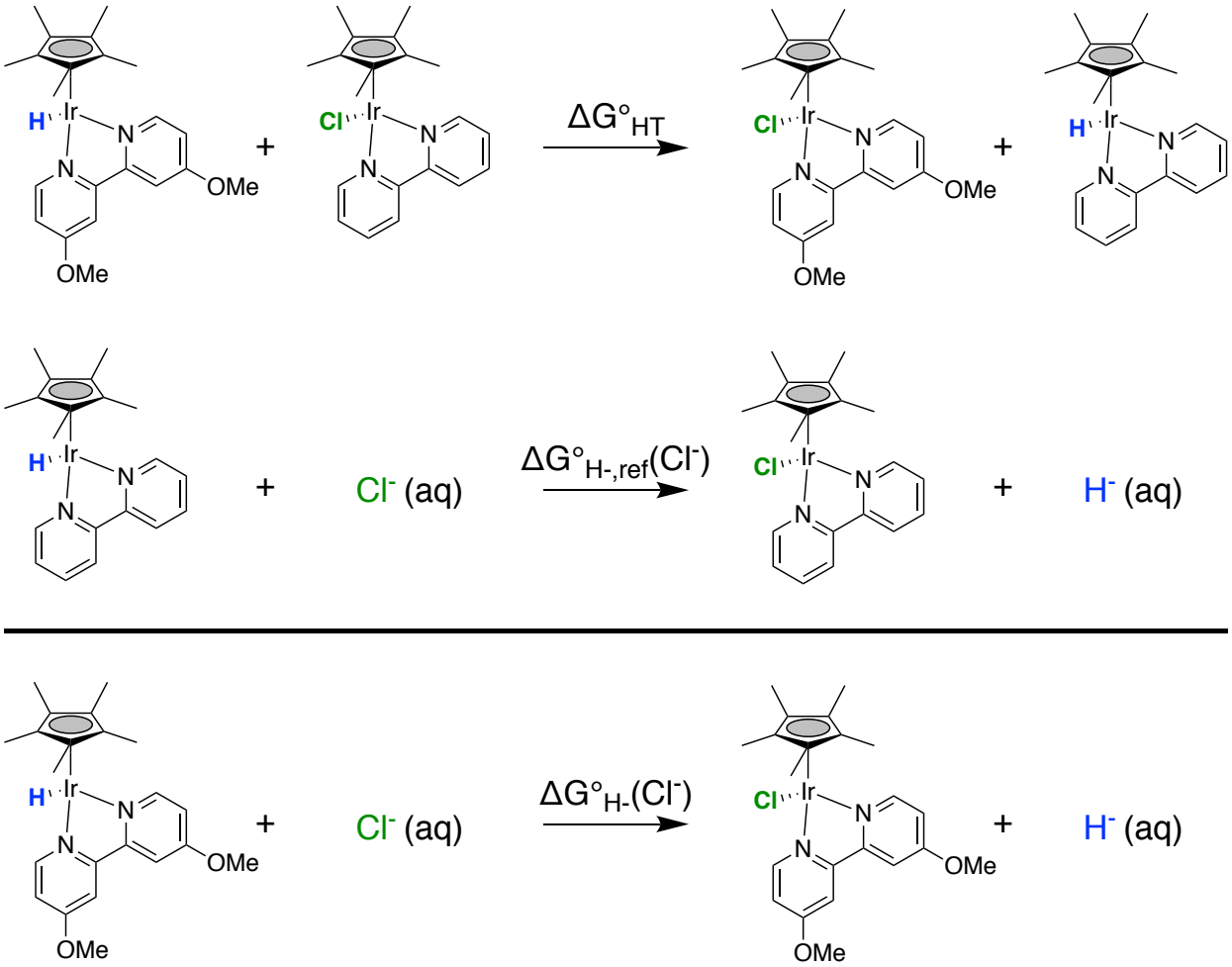

Figure S4. Illustrative reaction scheme for the computation of $\Delta G°_{H-}(Cl^-)$ for the methoxy substituted bpy complex. The DFT-computed $\Delta G°_{HT}$ was -0.8 kcal/mol, and the experimental reference $\Delta G°_{H-,ref}(Cl^-)$ was 27.0 kcal/mol. This gave a final hydricity value of $\Delta G°_{H-}(Cl^-)$ = 26.2 kcal/mol for the methoxy substituted complex.

Total Charge of Systems: The dipole moment of a charged system, and therefore the energy of a charged system in an external electric field, is ill-defined and depends on one's choice of origin. This can be shown using the definition of a dipole moment

$$\boldsymbol{\mu} = \int \boldsymbol{r}\rho(\boldsymbol{r})\, d\boldsymbol{r}$$

where $\boldsymbol{\mu}$ is the dipole moment, $\boldsymbol{\rho}$ is the charge density, and $\boldsymbol{r}$ is the displacement from the origin. If the origin is displaced by $\boldsymbol{r}_{dis}$, the resultant coordinate system has $\boldsymbol{r'} = \boldsymbol{r} - \boldsymbol{r}_{dis}$, $\rho'(\boldsymbol{r'}) = \rho(\boldsymbol{r})$, and $d\boldsymbol{r'} = d\boldsymbol{r}$. This gives an expression for the new dipole moment $\boldsymbol{\mu'}$:

$$\boldsymbol{\mu}' = \int \boldsymbol{r}'\rho(\boldsymbol{r})\, d\boldsymbol{r} = \int (\boldsymbol{r} - \boldsymbol{r}_{dis})\rho(\boldsymbol{r})\, d\boldsymbol{r}$$
$$\boldsymbol{\mu}' = \int \boldsymbol{r}\rho(\boldsymbol{r})\, d\boldsymbol{r} - \boldsymbol{r}_{dis}\int \rho(\boldsymbol{r})\, d\boldsymbol{r}$$
$$\boldsymbol{\mu}' = \boldsymbol{\mu} - Q\boldsymbol{r}_{dis}$$

The dipole moment of a neutral molecule ($Q = 0$) is unaffected by the change in origin, but the dipole moment depends on the origin for total charge $Q \neq 0$. This also results in a change to the first order shift of the total energy of the system:

$$\boldsymbol{E}' = -\boldsymbol{\mu}' \cdot \boldsymbol{F}$$
$$\boldsymbol{E}' = -\boldsymbol{\mu} \cdot \boldsymbol{F} + Q\boldsymbol{r}_{dis} \cdot \boldsymbol{F}$$

Thus, the energy of a charged system in a field depends on the choice of origin. If the total charge Q of the system does not change (as is the case for the reaction in this study), the origin should be kept constant between calculations so that the origin-dependent term cancels out between reactants and products.

The Ir bipyridyl complexes considered in this work have a positive total charge. Thus, it was important to verify that our calculations in an external electric field were not significantly affected by the fact that some systems had a net charge. This was verified by adding an extra electron to reduce the gold surface and neutralize the total charge. These results were very similar to those reported in the manuscript. Further details about these control calculations is provided in **Section S11**.

For calculations of charged molecules, all values are reported with the origin in the z-direction defined as the plane of the Au surface. The origin in the x and y directions do not affect the computed energies, as the external field is applied only in the z-direction ($-\boldsymbol{\mu} \cdot \boldsymbol{F} = -\boldsymbol{\mu}_z\boldsymbol{F}_z$). The results in **Section S11** demonstrate that the effect of this term is very small and support the use of calculations of charged systems with the origin at the surface plane.

Note that the field-dependent energy of a charged molecule at an interface should also formally include a QV term, where V is the electric potential difference between the surface and the solution. In this study, the reactants and products of each reaction have the same total charge Q, as a H^- ligand is exchanged for a Cl^-. Additionally, the orientation of the Ir-H reactants and Ir-Cl products are very similar, suggesting that there should be no major change in monolayer structure that would affect the relationship between V and F. Thus, there is need to add any

additional corrections to the DFT-computed values. However, this term should be considered in future studies of reactions involving charged species if there are changes in total charge or monolayer structure.

Calculations Without Gold Surface: To examine the perturbative effect of the field in the absence of the gold surface, it was essential to maintain the orientation of the complexes with respect to the field as well as the conformational distortions arising from adsorbate-surface interactions. This eliminated specific Au-thiolate interactions while maintaining the through-space effects of the field on the complexes. Four atoms were constrained to maintain the structure and orientation of the complex while allowing for the geometry optimizations needed for calculations of hydricity (free energies). Specifically, the sulfur, the two bound atoms from the chelating ligand (bpy or ppy), and one of the Cp* carbon atoms were frozen. An example of the constraints for **[Ir-bpy-H]**$^+$ is shown below in **Figure S5**. These calculations were not intended to describe the behavior of the catalyst in solution, which would be different due to the surface-induced geometric distortions, but were only used to see if there were field-dependent interactions between the adsorbate and Au surface.

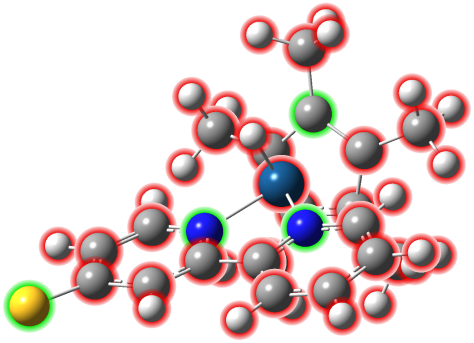

Figure S5. Constraints used for calculations of **[Ir-bpy-H]**$^+$ in the absence of a gold surface. Constrained atoms are indicated with a green outline.

Section S3 - Benchmarking of Hydricity Calculations

To ensure the accuracy of the computed hydricity values, we benchmarked our computational methods using the experimentally measured hydricity values for a series of **[Ir-bpy-H]**$^+$ analogues (**Figure S6**).[11] Hydricities were computed using the thermodynamic cycle method described in **Section S1**, with the unsubstituted complex serving as a reference (**Figure S3-4**). Several methods were considered for single point calculations in a water SMD continuum solvation model.[14] The ωB97-XD[15] functional and PBE[7] functional with Grimme's D3-BJ dispersion correction[8, 9] were found to reproduce the experimental trends in hydricity. Therefore, these two functionals were considered with two different mixed basis sets. Basis Set 1 (BS1) consisted of the 6-31+G(d,p) basis set[16-18] on nonmetal atoms and Def2SVP basis set and pseudopotential[19] on Ir. Basis Set 2 (BS2) consisted of the same 6-31+G(d,p) basis set on nonmetal atoms but the LANL2DZ[20] basis set with an additional *f* function on Ir, as had previously been recommended for iridium-mediated reactions using PBE-D functionals.[21] The ωB97-XD functional was chosen because it had the lowest error in predicting hydricity values (MAE = 0.23 kcal/mol). The change from BS1 to BS2 had negligible effect on the hydricities, so BS1 was chosen due to the additional polarization

functions on Ir (see **Tables S1-S4**). Larger basis sets were also tested with negligible changes in the computed energy differences, but were excluded due to difficult SCF convergence for the surface-attached systems with external electric fields.

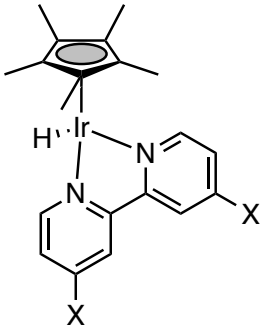

Figure S6: Complexes used for benchmarking had symmetric substituents in positions X

Table S1: Computed Hydricities with ωB97-XD functional and BS1 (MAE = 0.23 kcal/mol)

Substituent	**Computed $\Delta G°_{H-}(Cl^-)$** [kcal/mol]	**Measured $\Delta G°_{H-}(Cl^-)$** [kcal/mol]
CO_2^-	27.7	27.6
COOMe	28.0	28.6
Me	26.4	26.6
OMe	26.2	26.2

Table S2: Computed Hydricities with ωB97-XD functional and BS2 (MAE = 0.25 kcal/mol)

Substituent	**Computed $\Delta G°_{H-}(Cl^-)$** [kcal/mol]	**Measured $\Delta G°_{H-}(Cl^-)$** [kcal/mol]
CO_2^-	27.7	27.6
COOMe	27.9	28.6
Me	26.4	26.6
OMe	26.2	26.2

Table S3: Computed Hydricities with PBE functional and BS1 (MAE = 0.40 kcal/mol)

Substituent	**Computed $\Delta G°_{H-}(Cl^-)$** [kcal/mol]	**Measured $\Delta G°_{H-}(Cl^-)$** [kcal/mol]
CO_2^-	27.1	27.6
COOMe	28.7	28.6
Me	26.2	26.6
OMe	25.6	26.2

Table S4: Computed Hydricities with PBE functional and BS2 (MAE = 0.40 kcal/mol)

Substituent	**Computed $\Delta G°_{H-}(Cl^-)$** [kcal/mol]	**Measured $\Delta G°_{H-}(Cl^-)$** [kcal/mol]
CO_2^-	27.1	27.6
COOMe	28.7	28.6
Me	26.2	26.6
OMe	25.6	26.2

Section S4 - Field-Dependent Hydricity Values

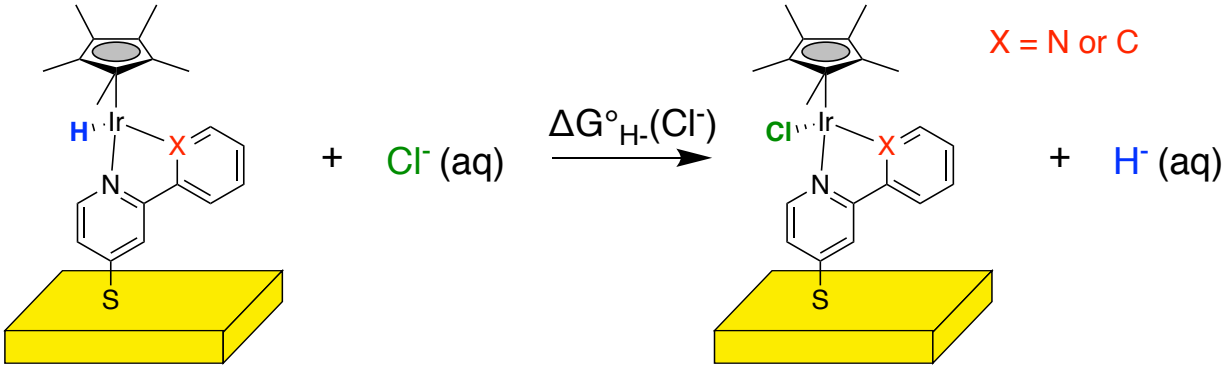

Figure S7. Reaction scheme for the effective hydricities, $\Delta G°_{H^-}(Cl^-)$, of **[Ir-bpy-H]**$^+$ and **Ir-ppy-H** which were studied as a function of electric field strength.

Table S5: Field-Dependent Hydricities of Surface Attached Complexes

Field [V/nm]	$\Delta G°_{H^-}(Cl^-)$ [Ir-bpy-H]$^+$ [kcal/mol]	$\Delta G°_{H^-}(Cl^-)$ Ir-ppy-H [kcal/mol]
-1.03	24.2	21.3
-0.77	24.6	21.4
-0.51	25.1	21.8
-0.26	25.5	22.2
0	25.8	22.7
+0.26	26.0	23.2
+0.51	26.2	23.8
+0.77	26.8	23.9
+1.03	27.1	24.6

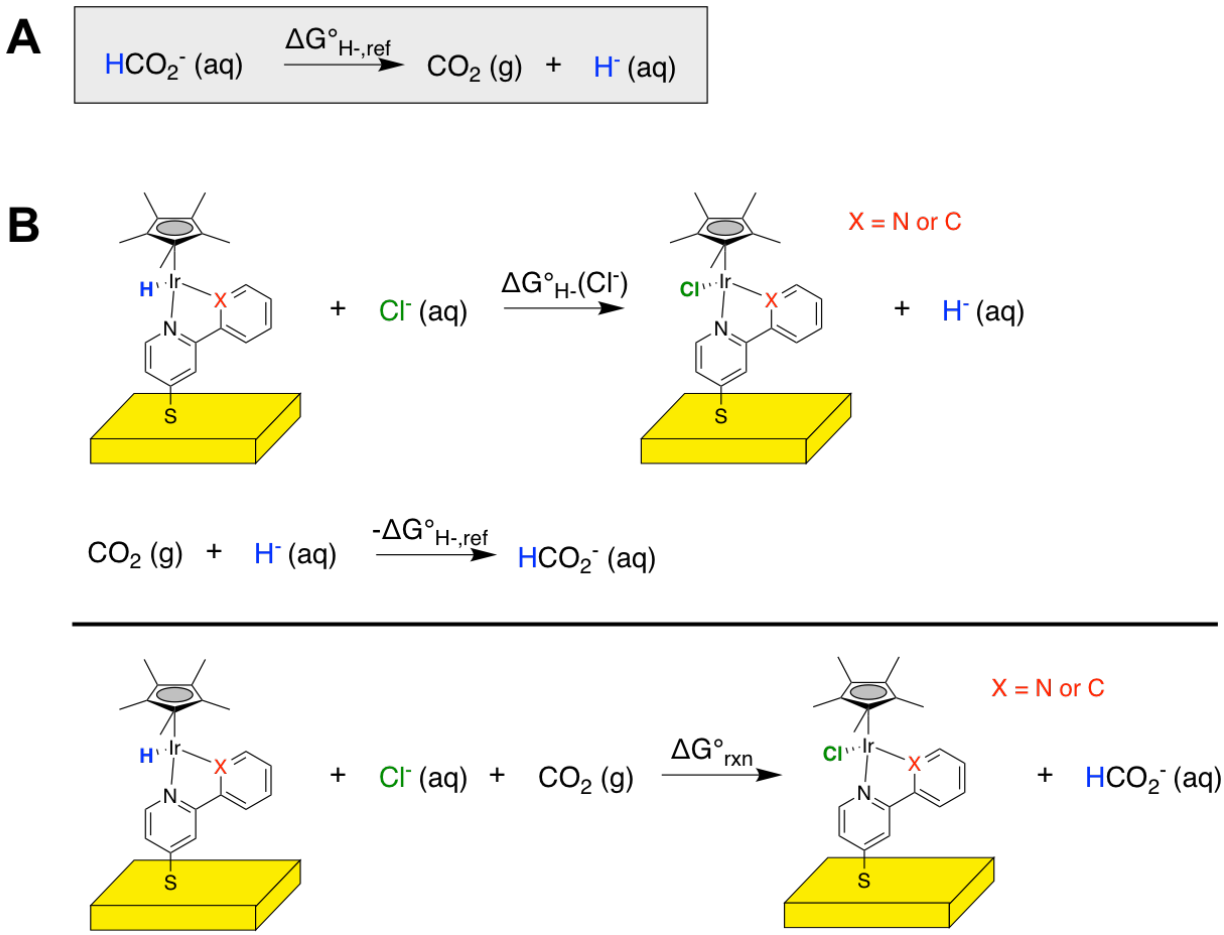

Figure S8. Reaction scheme for determining the thermodynamic favorability of hydride transfer from the surface-attached complexes to CO_2 to produce formate. The computed field-dependent $\Delta G°_{H-}(Cl^-)$ values of **[Ir-bpy-H]**$^+$ and **Ir-ppy-H** can be combined with the reported aqueous hydricity of formate, $\Delta G°_{H-,ref}$ (24.1 kcal/mol)[22] to predict whether the hydride transfer is thermodynamically favorable ($\Delta G°_{rxn}$).

Section S5 – Evaluation of Higher Spin States

One possible effect of an external electric field is the stabilization of higher spin states on the metal center. To investigate this possibility, triplet spin states were calculated for each intermediate at all field strengths. For computational efficiency and to eliminate spurious high-spin states involving unpaired Au electrons, the Au surface was excluded in these calculations. In all cases, the triplet state was found to be at least 35 kcal/mol higher in energy than the corresponding singlet (**Table S6**), so stabilization of high-spin states is not relevant in these systems.

Table S6. Free energy difference between triplet and singlet states at each field strength. The triplet state is unfavorable for all molecules at all field strengths.

Field Strength [V/nm]	$[Ir\text{-}bpy\text{-}H]^+$ [kcal/mol]	$[Ir\text{-}bpy\text{-}Cl]^+$ [kcal/mol]	Ir-ppy-H [kcal/mol]	$[Ir\text{-}ppy\text{-}Cl]^+$ [kcal/mol]
-1.03	+45.8	+44.0	+48.7	+35.0
-0.77	+46.1	+44.3	+48.7	+35.5
-0.51	+46.3	+42.6	+55.3	+35.9
-0.26	+46.6	+42.8	+54.7	+36.3
0	+46.9	+43.1	+54.0	+36.8
+0.26	+47.1	+43.4	+53.4	+37.3
+0.51	+47.3	+43.4	+52.6	+37.8
+0.77	+47.5	+43.7	+51.9	+38.2
+1.03	+47.8	+44.0	+51.2	+38.9

Section S6 - Dipole Moments

Consideration of the dipole moments for these complexes needs to be done carefully, as the bipyridyl species have a net positive charge. As discussed in **Section S1**, species with a net charge do not have well-defined dipole moments; the value of the dipole moment depends on the choice of origin. However, the dipole moment serves as a useful quantity both for estimating shifts in energy due to an applied field and for understanding the underlying cause of these shifts. The only relevant component of the dipole moment is that which aligns with the applied field (z-component), so we have only reported μ_z for each species. The reported μ_z values for all charged species are relative to an origin defined as the Au surface plane. To justify the use of these dipole moments, we have also performed calculations with extra electron(s) added to the gold surface to give the system a neutral charge (**Section S11**). Values for μ_z computed via the two methodologies are very similar, suggesting that the μ_z values for the charged species can be used for predictions of energy shifts. This confirmation is particularly important for future computational studies that may not contain metal electrodes that can accommodate extra electrons; the results suggest that dipole moments for charged systems can still be used for valuable predictions as long as the origin is kept constant and the reaction does not change the total charge of the system.

Several sets of dipole moment component μ_z are provided for the complexes optimized on a gold electrode surface. These include: μ_z values for the complexes on the gold surface (**Table 1**), μ_z for the complexes alone in their surface-optimized geometries but without the surface (**Table S7**), and μ_z for the complexes following the constrained optimization described in **Section S2** (**Table S8**). It is notable that the change in μ_z upon replacing the hydride with chloride is similar in all cases, helping to explain why the perturbative effect of the field changes very little in the absence of the gold surface (**Figure 6**).

Table S7: Projection of dipole moment along the field axis (μ_z) fo the complexes in their surface-optimized geometries without the Au surface. $\Delta\mu_z$ is -3.4 D for the bpy complex and -5.6 D for the ppy complex.

Species	μ_z [D]
[Ir-bpy-H]$^+$	6.0
[Ir-bpy-Cl]$^+$	2.6
Ir-ppy-H	-11.8
Ir-ppy-Cl	-17.4

Table S8: Projection of dipole moment along the field axis (μ_z) for complexes after constrained optimization without the Au surface. $\Delta\mu_z$ is -3.0 D for the bpy complex and -4.3 D for the ppy complex.

Species	μ_z [D]
[Ir-bpy-H]$^+$	4.7
[Ir-bpy-Cl]$^+$	1.7
Ir-ppy-H	-13.5
Ir-ppy-Cl	-17.8

Section S7 – Using Dipole Moments to Predict Field Control of Reaction Thermodynamics

The dipole moments of reactants and products can be used to make an estimate of how the thermodynamics of a chemical reaction is controlled by an applied field. The total electronic energy, E, of a molecule in an applied field, $\boldsymbol{F}$, is given by the Taylor series:

$$E = E_0 - \left[\frac{\partial E}{\partial \boldsymbol{F}}\right]_{F=0} \cdot \boldsymbol{F} + \frac{1}{2}\left[\frac{\partial^2 E}{\partial \boldsymbol{F}^2}\right]_{F=0} \boldsymbol{F}^2 + \ldots$$
$$E = E_0 - \boldsymbol{\mu} \cdot \boldsymbol{F} + \frac{1}{2}\boldsymbol{\alpha}\boldsymbol{F}^2 + \ldots$$

where E_0 is the total energy, $\boldsymbol{\mu}$ is the dipole moment, and $\boldsymbol{\alpha}$ is the polarizability. All three of these quantities are determined for the molecule in the absence an applied field. The total electronic energy change associated with a chemical reaction is given by:

$$\Delta E = \sum E_{products} - \sum E_{reactants}$$

In our study, there is only one reactant (the Ir-H species) and one product (the Ir-Cl species) which is affected by the applied electric field. Additionally, the shifts in ΔE are linear which suggests that the reactants and products have similar polarizabilities. Thus, we can approximate the effect of the applied field on the reaction energetics as:

$$\Delta E \approx E_{0,Ir-Cl} - E_{0,Ir-H} - (\boldsymbol{\mu}_{Ir-Cl} - \boldsymbol{\mu}_{Ir-H}) \cdot \boldsymbol{F} = \Delta E_0 - \Delta\boldsymbol{\mu} \cdot \boldsymbol{F}$$

For all calculations, the field is applied perpendicular to the electrode surface (along z-axis). Therefore, only the z-component of the dipole moment interacts with the applied field, giving:

$$\Delta E - \Delta E_0 \approx -\Delta\mu_z F_z$$

By taking the zero-field structure of the reactants and products and calculating $\Delta E - \Delta E_0$ as a function of Fz, we show explicitly that the slope equals $-\Delta\mu_{z,}$ (**Figure S9**). This reveals the precise meaning of the energy shifts predicted from the dipole moments, and provides guidance for when they can be used to predict the field dependence of the reaction thermodynamics (ΔG). Using $-\Delta\mu_z$ to predict energy shifts neglects the effect of any changes in molecular structure or orientation that occur when a field is applied. Furthermore, the Gibbs free energy includes not only the total electronic energy E, but also the zero-point energy and various thermal corrections. If these structural and thermal effects are small, $-\Delta\mu_z$ will provide good estimates of the shifts in the Gibbs free energy of a reaction.

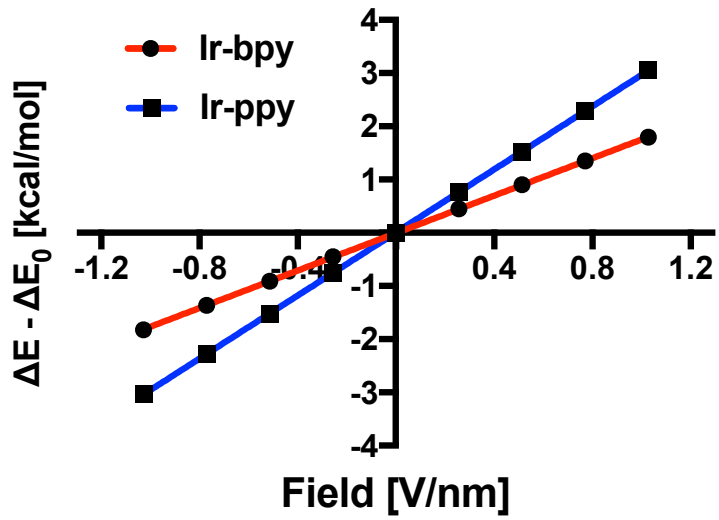

Figure S9. Shift in the total electronic energy of the hydride transfer reaction for **[Ir-bpy-H]**$^+$ and **Ir-ppy-H** ($\Delta E - \Delta E_0$) as a function of the applied electric field with best-fit lines of +1.8 and +3.0 kcal mol^{-1}/V nm^{-1}, respectively ($R^2 > 0.99$ for both fits). The molecules are constrained in their zero-field geometries, and the total energy is calculated in the presence of an external field. The slopes of these lines correspond exactly to $-\Delta\mu_z$ (3.6 D for **[Ir-bpy-H]**$^+$, 6.1 D for **Ir-ppy-H**), showing that the slightly smaller hydricity slopes result from structural relaxation and thermochemical effects that are excluded here.

Section S8 – Vibrational Analysis

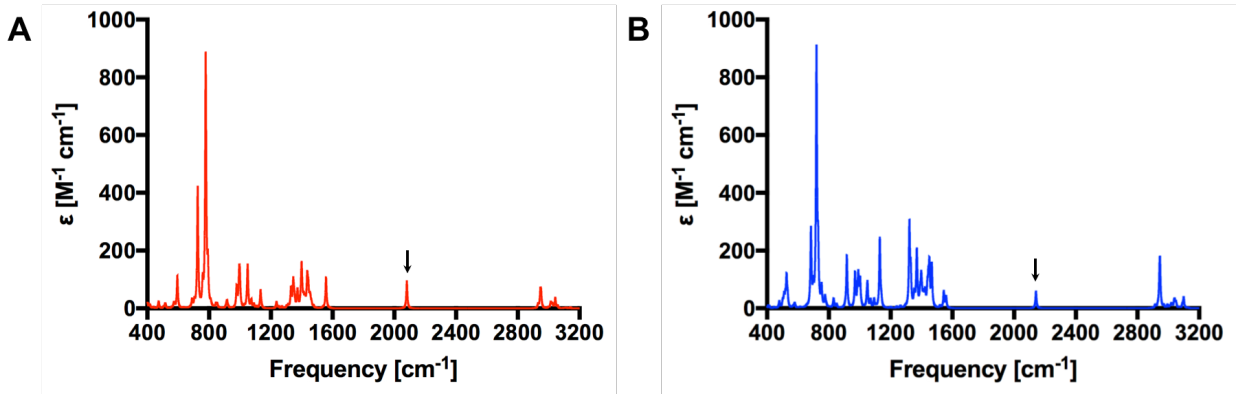

Figure S10. Computed IR spectra for (A) **[Ir-bpy-H]**$^+$ and (B) **Ir-ppy-H** showing all transitions above 400 cm^{-1}. The peaks corresponding to the Ir-H stretching mode are marked with a black arrow. In both cases, the Ir-H stretch is well separated from all other vibrational modes.

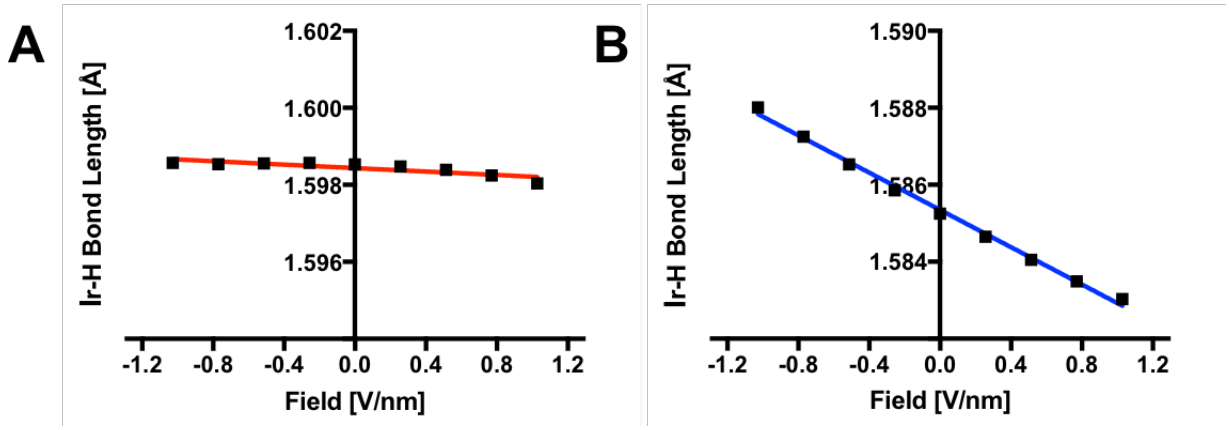

Figure S11. Ir-H bond lengths of (A) **[Ir-bpy-H]**$^+$ and (B) **Ir-ppy-H** as a function of the applied electric field. The slope of the best fit line for **Ir-ppy-H** was -2.4×10^{-3} Å/V nm^{-1} (R^2>0.99). The line of best fit for **[Ir-bpy-H]**$^+$ is shown only to guide the eye; the changes in Ir-H bond length are an order of magnitude smaller and nonlinear, and such small changes are likely insignificant.

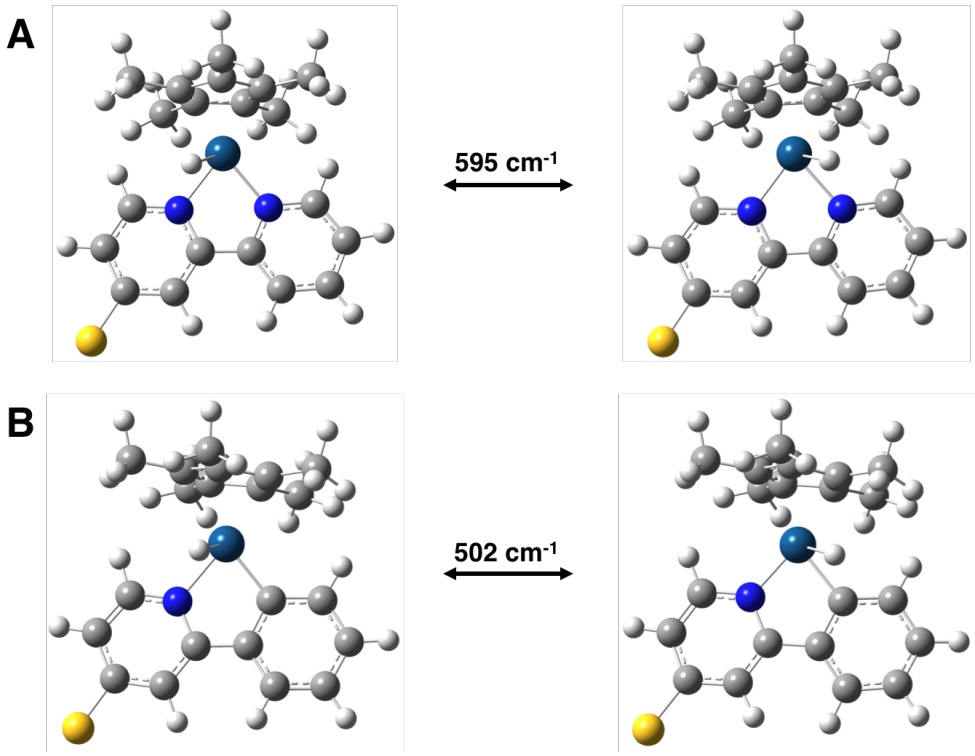

Figure S12. Visualization of the Ir-H wagging mode of (A) **[Ir-bpy-H]**$^+$ and (B) **Ir-ppy-H** with the corresponding vibrational frequency indicated.

Section S9 – Comparison with Substituted Complexes

Table S9: DFT-computed aqueous hydricities of Ir-bpy complexes with symmetric 4,4′ chemical substituents with varying Hammett parameters (σ_p^-)

Substituent	σ_p^-	$\Delta G°_{H^-}(Cl^-)$ [kcal/mol]
OH	-0.37	26.4
OMe	-0.26	26.2
Me	-0.17	26.4
tBu	-0.13	26.7
H	0.0	27.0
CO_2^-	0.31	27.7
CF_3	0.65	28.1
COOMe	0.75	28.0
CN	1	28.4
NO_2	1.27	28.9

Table S10: DFT-computed aqueous hydricities of Ir-ppy complexes with symmetric 4,4′ chemical substituents with varying Hammett parameters (σ_p^-)

Substituent	σ_p^-	$\Delta G°_{H^-}(Cl^-)$ [kcal/mol]
OH	-0.37	25.5
OMe	-0.26	25.5
Me	-0.17	25.9
tBu	-0.13	26.1
H	0.0	25.8
CO_2^-	0.31	26.7
CF_3	0.65	28.0
COOMe	0.75	27.5
CN	1	27.8
NO_2	1.27	28.5

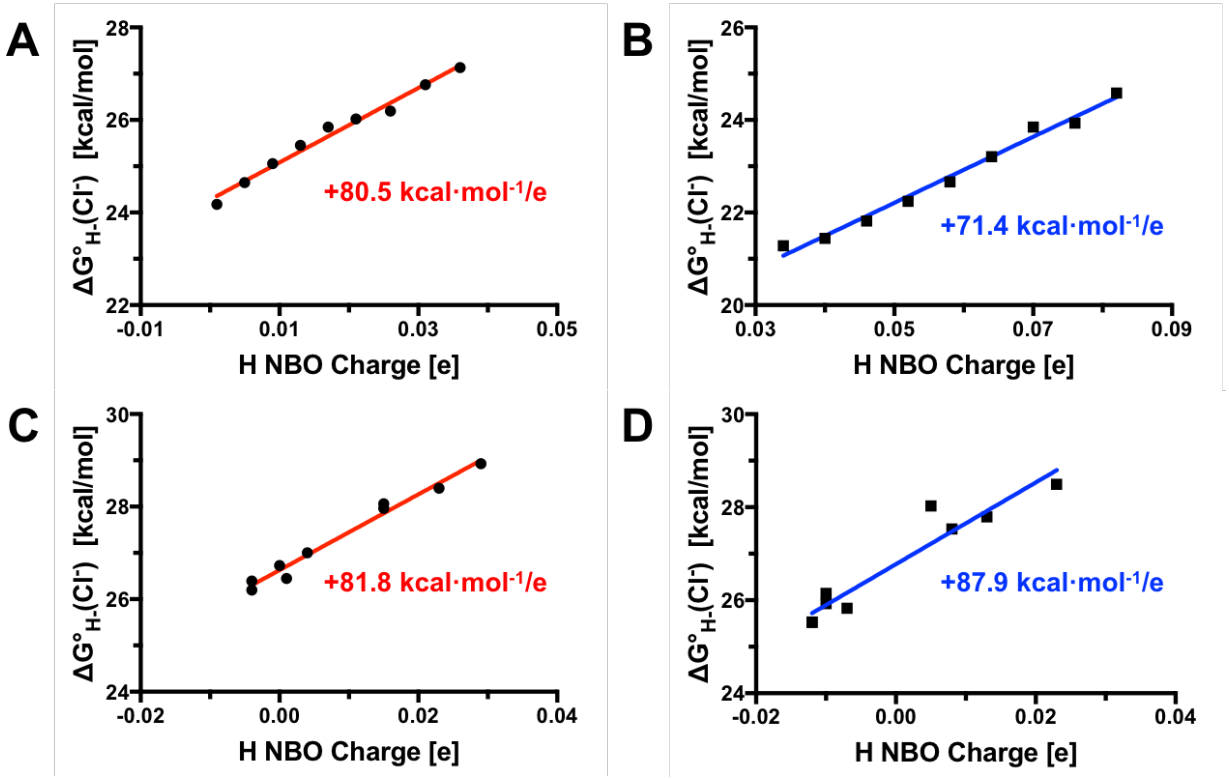

Figure S13. Correlation between the NBO partial charge on the hydridic H atom and the hydricity of surface-attached (A) **[Ir-bpy-H]**$^+$ and (B) **Ir-ppy-H** complexes as an electric field is applied. The same correlation was also analyzed for the chemically substituted (C) Ir-bpy and (D) Ir-ppy complexes. The slopes of $\Delta G°_{H^-}(Cl^-)$ *vs* the partial charge on the H atom are shown for the linear fit of each graph ($R^2 > 0.98$ for A, B, and C; $R^2 = 0.91$ for D).

Section S10 – Local Electrostatic Analysis

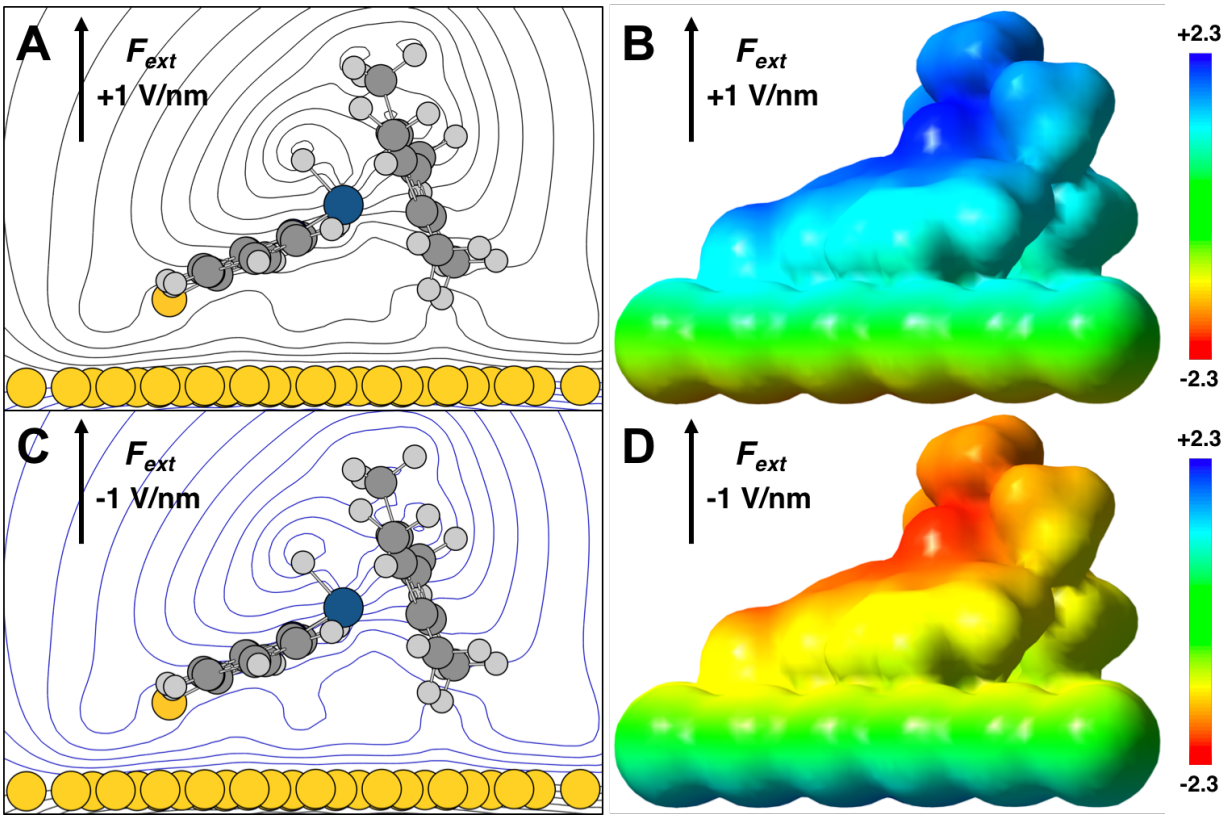

Figure S14. Contour maps of the difference in ESP after applying fields of (A) +1 V/nm and (C) -1 V/nm to **Ir-ppy-H**. Lines are spaced by units of 0.002 a.u. = 0.054 V, with black lines for positive and blue lines for negative values. Potential difference values mapped onto an electron density surface (isovalue = 0.005 a.u) for fields of (B) +1 V/nm and (D) -1 V/nm. A bar is included to show the color scaling in units of 10^{-2} a.u.

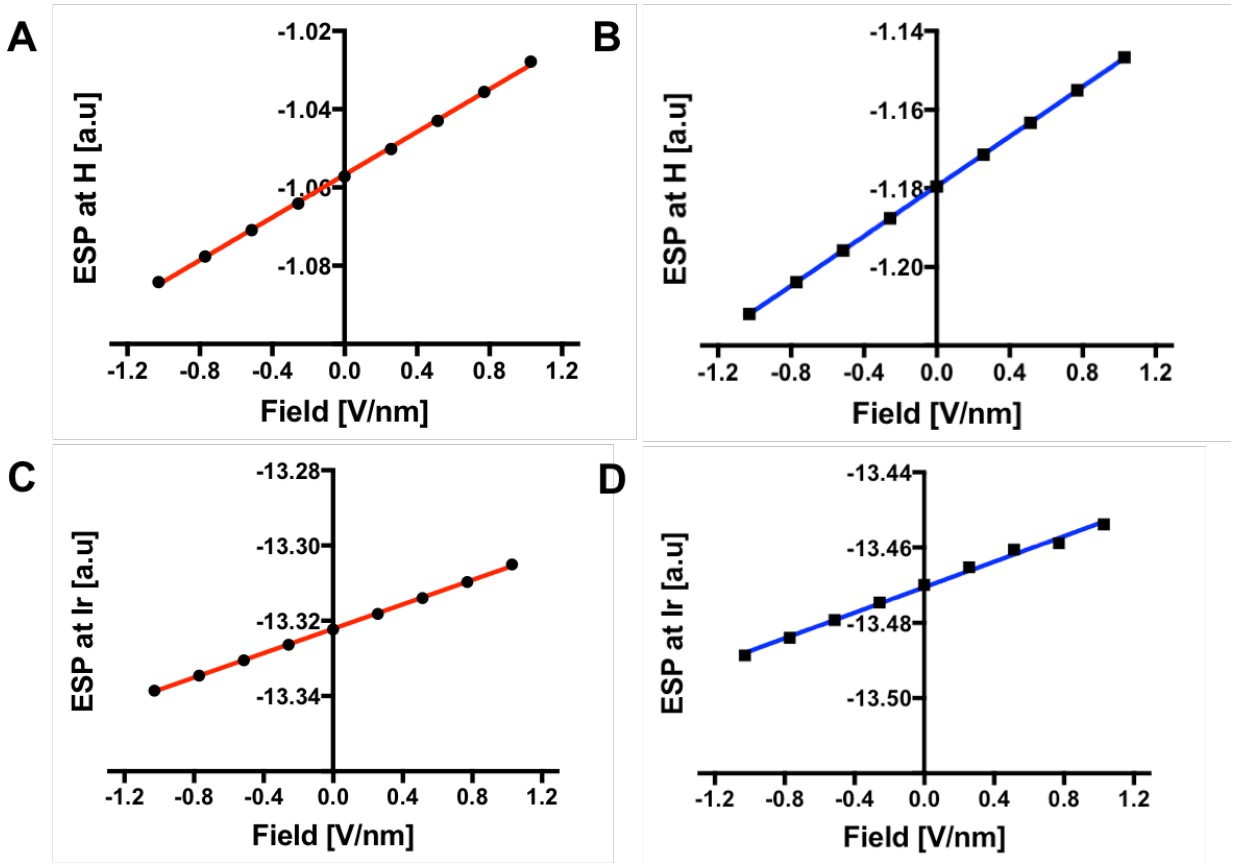

Figure S15. ESP at the hydridic H atom for (A) **[Ir-bpy-H]**$^+$ and (B) **Ir-ppy-H** and ESP at the Ir atom for (C) **[Ir-bpy-H]**$^+$ and (D) **Ir-ppy-H** as a function of the applied electric field. The slopes of the best fit lines were (A) $+2.7\times10^{-3}$ a.u./V nm^{-1}, (B) $+3.2\times10^{-3}$ a.u./V nm^{-1}, (C) $+1.6\times10^{-3}$ a.u./V nm^{-1}, and (D) $+1.7\times10^{-3}$ a.u./V nm^{-1} (all $R^2 > 0.99$). Changes in the ESP at the hydridic H atom were larger than those at any other atom for both complexes.

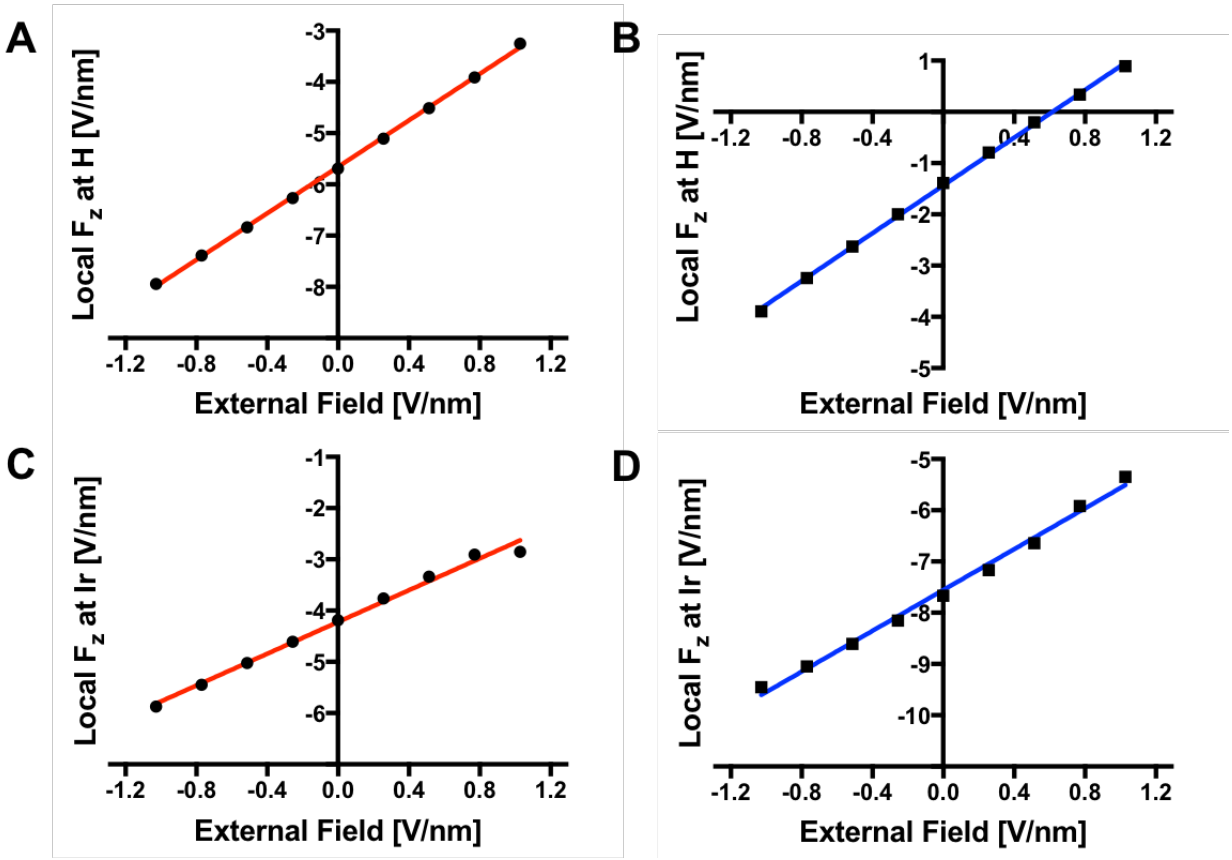

Figure S16. Z-component of the local electric field (F_z) at the hydridic H atom of (A) **[Ir-bpy-H]**$^+$ and (B) **Ir-ppy-H** and F_z at the Ir atom for (C) **[Ir-bpy-H]**$^+$ and (D) **Ir-ppy-H** as a function of the applied external electric field. These values combine the field arising from the electrons/nuclei of the molecule with the effect of the external field. The slopes of the best fit lines were (A) +2.27, (B) +2.33, (C) +1.55, and (D) +1.99 (all $R^2 > 0.99$). All slopes are larger than 1, indicating that changes in the electron density and nuclear positions work with the external field to amplify the local field at the H and Ir atoms. Changes in F_z at the hydridic H atom were larger than those at any other atom for both complexes.

Section S11 – Control Calculations with Neutralized Systems

Since the energies and dipole moments of charged systems in a field depend on the choice of origin (**Section S1**), the calculations for the charged Ir-bpy systems were repeated with an extra electron added to the gold surface to neutralize the total charge (i.e. a negatively charged gold surface). These control calculations were performed to ensure that there were no major changes from the results with the charged systems. First, single point energy calculations were performed to see if there was any significant change to the resulting dipole moments (**Table S11**). The changes in μ_z were small (< 0.2 D), supporting the use of the values computed for the charged species and that the Au-surface was a meaningful choice of origin.

We also confirmed that the "neturalized" systems observe the same changes in hydricity as the charged ones. It was necessary to perform optimizations for each of the neutral systems to enable the computation of free energy changes (frequency calculations need to be performed at a stationary point). These optimized species showed larger changes in μ_z than the single point calculations, since interactions between the positively charged molecules and the negatively charged Au surface resulted in small changes in molecular geometry (**Table S12**). Correspondingly, the changes in hydricity were slightly larger for the neutralized systems due to these small conformational changes (**Figure S17, Table S13**).

Table S11: z-Components of dipole moments of the complexes attached to the Au surface. Dipole moments of "neutralized" systems were computed from single point calculations of the charged geometries with an extra electron added to the Au surface to achieve a neutral total charge.

Species	μ_z (Charged) **[D]**	μ_z (Neutralized) **[D]**
[Ir-bpy-H]$^+$	10.9	10.9
[Ir-bpy-Cl]$^+$	7.3	7.1

Table S12: z-Components of dipole moments of the complexes attached to the Au surface. Dipole moments of "neutralized" systems were computed from geometry optimization of the complexes on the negatively charged Au surfaces (neutral total charge).

Species	μ_z (Charged) **[D]**	μ_z (Neutralized) **[D]**
[Ir-bpy-H]$^+$	10.9	10.6
[Ir-bpy-Cl]$^+$	7.3	6.8

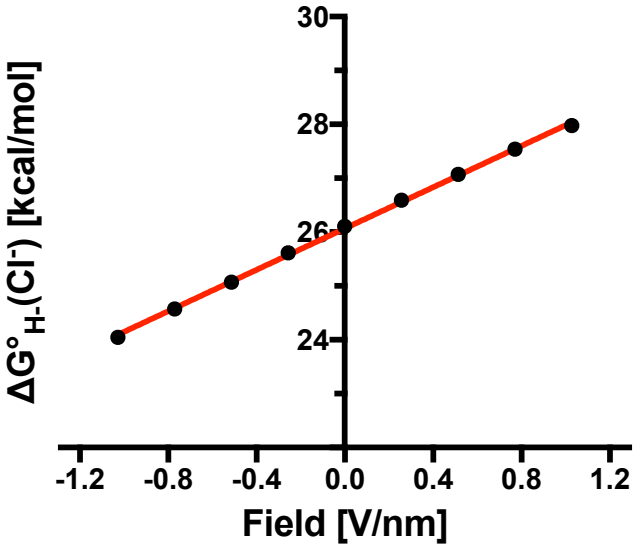

Figure S17: Hydricity values of complexes **[Ir-bpy-H]**$^+$ (neutralized system) as a function of the applied electric field with a best-fit line with a slope of +1.9 kcal mol^{-1}/ V nm^{-1} ($R^2 > 0.99$), which is comparable to the value of +1.4 kcal mol^{-1}/ V nm^{-1} obtained for the charged system.

Table S13: Field-dependent hydricities of charged and neutralized Au-attached **[Ir-bpy-H]**$^+$ systems

Field [V/nm]	**$\Delta G°_{H-}(Cl^-)$ (charged) [kcal/mol]**	**$\Delta G°_{H-}(Cl^-)$ (neutral) [kcal/mol]**
-1.03	24.2	24.0
-0.77	24.6	24.6
-0.51	25.1	25.1
-0.26	25.5	25.6
0	25.8	26.1
+0.26	26.0	26.6
+0.51	26.2	27.1
+0.77	26.8	27.5
+1.03	27.1	28.0

Section S12 – References

1. Kresse, G.; Hafner, J. Ab Initio Molecular Dynamics for Liquid Metals. *Phys. Rev. B* **1993,** *47*, 558-561.
2. Kresse, G.; Hafner, J. Ab Initio Molecular-Dynamics Simulation of the Liquid-Metal – Amorphous-Semiconductor Transition in Germanium. *Phys. Rev. B* **1994,** *49*, 14251-14269.
3. Kresse, G.; Furthmüller, J. Efficiency of Ab-Initio Total Energy Calculations for Metals and Semiconductors Using a Plane-Wave Basis Set. *Comput. Mater. Sci.* **1996,** *6*, 15-50.
4. Kresse, G.; Furthmüller, J. Efficient Iterative Schemes for Ab Initio Total-Energy Calculations Using a Plane-Wave Basis Set. *Phys. Rev. B* **1996,** *54*, 11169-11186.
5. Blöchl, P. E. Projector Augmented-Wave Method. *Phys. Rev. B* **1994,** *50*, 17953-17979.
6. Kresse, G.; Joubert, D. From Ultrasoft Pseudopotentials to the Projector Augmented-Wave Method. *Phys. Rev. B* **1999,** *59*, 1758-1775.
7. Perdew, J. P.; Burke, K.; Ernzerhof, M. Generalized Gradient Approximation Made Simple. *Phys. Rev. Lett.* **1996,** *77*, 3865-3868.
8. Grimme, S.; Antony, J.; Ehrlich, S.; Krieg, H. A Consistent and Accurate Ab Initio Parametrization of Density Functional Dispersion Correction (DFT-D) for the 94 Elements H-Pu. *J. Chem. Phys.* **2010,** *132*, 154104.
9. Grimme, S.; Ehrlich, S.; Goerigk, L. Effect of the Damping Function in Dispersion Corrected Density Functional Theory. *J. Comput. Chem.* **2011,** *32*, 1456-1465.
10. Methfessel, M.; Paxton, A. T. High-Precision Sampling for Brillouin-Zone Integration in Metals. *Phys. Rev. B* **1989,** *40*, 3616-3621.
11. Pitman, C. L.; Brereton, K. R.; Miller, A. J. M. Aqueous Hydricity of Late Metal Catalysts as a Continuum Tuned by Ligands and the Medium. *J. Am. Chem. Soc.* **2016,** *138*, 2252-2260.
12. Chen, S.; Rousseau, R.; Raugei, S.; Dupuis, M.; DuBois, D. L.; Bullock, R. M. Comprehensive Thermodynamics of Nickel Hydride Bis(Diphosphine) Complexes: A Predictive Model Through Computations. *Organometallics* **2011,** *30*, 6108-6118.
13. Sandhya, K. S.; Suresh, C. H. Quantification of Thermodynamic Hydridicity of Hydride Complexes of Mn, Re, Mo, and W Using the Molecular Electrostatic Potential. *J. Phys. Chem.* **2017,** *121*, 2814-2819.
14. Marenich, A. V.; Cramer, C. J.; Truhlar, D. G. Universal Solvation Model Based on Solute Electron Density and on a Continuum Model of the Solvent Defined by the Bulk Dielectric Constant and Atomic Surface Tensions. *J. Phys. Chem. B* **2009,** *113*, 6378-6396.
15. Chai, J.-D.; Head-Gordon, M. Long-Range Corrected Hybrid Density Functionals with Damped Atom–Atom Dispersion Corrections. *Phys. Chem. Chem. Phys.* **2008,** *10*, 6615-6620.
16. Francl, M. M.; Pietro, W. J.; Hehre, W. J.; Binkley, J. S.; Gordon, M. S.; DeFrees, D. J.; Pople, J. A. Self-Consistent Molecular Orbital Methods. XXIII. A Polarization-Type Basis Set for Second-Row Elements. *J. Chem. Phys.* **1982,** *77*, 3654-3665.
17. Hariharan, P. C.; Pople, J. A. The Influence of Polarization Functions on Molecular Orbital Hydrogenation Energies. *Theor. Chim. Acta* **1973,** *28*, 213-222.
18. Clark, T.; Chandrasekhar, J.; Spitznagel, G. W.; Schleyer, P. V. R. Efficient Diffuse Function-Augmented Basis Sets for Anion Calculations. III. The 3-21+G Basis Set for First-Row Elements, Li–F. *J. Comput. Chem.* **1983,** *4*, 294-301.
19. Weigend, F. Accurate Coulomb-Fitting Basis Sets for H to Rn. *Phys. Chem. Chem. Phys.* **2006,** *8*, 1057-1065.

20. Hay, P. J.; Wadt, W. R. Ab Initio Effective Core Potentials for Molecular Calculations. Potentials for the Transition Metal Atoms Sc to Hg. *J. Chem. Phys.* **1985,** *82*, 270-283.
21. Hopmann, K. H. How Accurate is DFT for Iridium-Mediated Chemistry? *Organometallics* **2016,** *35*, 3795-3807.
22. Connelly, S. J.; Wiedner, E. S.; Appel, A. M. Predicting the Reactivity of Hydride Donors in Water: Thermodynamic Constants for Hydrogen. *Dalton Trans.* **2015,** *44*, 5933-5938.